CONFERENCES AND SYMPOSIA

PACS numbers: **01.10.–m**, 01.10.Fv, 72.25.Dc, **73.20.–r**, **73.40.–c**, 73.50.Pz

Topological states: what are they and what are they for?
(Scientific session of the Physical Sciences Division of the Russian Academy of Sciences, 29 November 2017)

DOI: https://doi.org/10.3367/UFNe.2017.11.038257

A scientific session of the Physical Sciences Division of the Russian Academy of Sciences (RAS) entitled "Topological states: what are they and what are they for?" was held on 29 November 2017 in the conference hall of the Lebedev Physical Institute, RAS.

The following reports were heard at the session:

(1) **Tarasenko S A** (Ioffe Institute, St. Petersburg) "Electron properties of topological insulators. The structure of edge states and photogalvanic effects";

(2) **Devyatov E V** (Institute of Solid State Physics, RAS, Chernogolovka, Moscow region) "Charge transfer between a superconductor and an edge-carrying state in an inverted band system";

(3) **Volkov V A** (Kotel'nikov Institute of Radio Engineering and Electronics, RAS, Moscow). "Surface states of Dirac and Weyl fermions".

The paper version of report 1 is presented further on in this issue.

Uspekhi Fizicheskikh Nauk **188** (10) 1129 – 1134 (2018)
DOI: https://doi.org/10.3367/UFNr.2017.11.038257
Translated by E G Strel'chenko; edited by A Radzig

PACS numbers: 72.25.Dc, **73.20.–r**, **73.40.–c**, 73.50.Pz
DOI: https://doi.org/10.3367/UFNe.2017.11.038351

Electron properties of topological insulators. The structure of edge states and photogalvanic effects

S A Tarasenko

Abstract. **Integrating the ideas of topology and topological transitions into solid-state physics has led to the theoretical prediction and subsequent experimental discovery of topological insulators, a new class of three- or quasi-two-dimensional dielectric crystalline systems exhibiting stable conducting surface states. This paper briefly reviews the electronic properties of topological insulators. The structure of edge and bulk electronic states in two- and three-dimensional HgTe-based topological insulators is described in particular detail. Recent theoretical and experimental results on the interaction of an electromagnetic field with topological insulators and on edge and surface photogalvanic effects are presented.**

Keywords: topological insulators, edge and surface states, photogalvanic effects

Contents

1. Introduction

Implementation of the ideas of topology and topological transitions in solid-state physics [1–4] led at the beginning of the 21st century to the theoretical prediction and the subsequent experimental discovery of topological insulators — a new class of three-dimensional (or quasi-two-dimensional) crystalline systems supporting stable conducting surface (or edge) states [5, 6]. Great attention on topological insulators is connected both with the fundamental interest in surface physics, which is very important in nanostructures, and with the prospects of using these systems to create new functional materials and devices for electronics and optoelectronics.

The appearance of states localized on a crystal surface or on the heterointerface between two materials is, at a phenomenological level, due to translational symmetry violation. The existence of such states was first theoretically predicted by I Y Tamm [7]. Later on, these states were discovered in various systems. The existence or absence of Tamm states and their properties in specific systems are mainly defined by the surface structure. Surface and edge states in topological insulators are quite extraordinary. They are stable with respect to impurities and inhomogeneities of the surface and fill the whole bandgap of a bulk crystal. These states are defined by the band structure topology of a bulk crystal and not by the specific morphology of the surface [5, 6, 8, 9]. 'Topologically protected' surface and edge states can form in insulating materials with an inverted band structure caused by strong spin-orbit coupling. The band structure of any insulating crystal can be characterized by the topological invariants Z_2, which take either 0 or 1 values and define which insulator type the specific crystal is attributed to: trivial or nontrivial.

S A Tarasenko Ioffe Institutes,
ul. Politekhnicheskaya 26, 194021 St. Petersburg, Russian Federation
E-mail: tarasenko@coherent.ioffe.ru

Received 16 April 2018
Uspekhi Fizicheskikh Nauk **188** (10) 1129 – 1134 (2018)
DOI: https://doi.org/10.3367/UFNr.2017.11.038351
Translated by A L Chekhov; edited by A Radzig

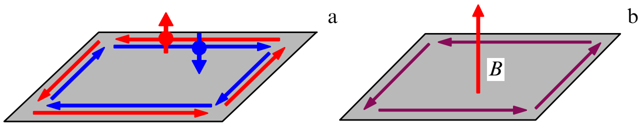

Figure 1. (a) Two-dimensional topological insulator with the Z_2 invariant. The system has the geometry of the quantum spin Hall effect with helical edge states. (b) An example of a topological insulator with the Z invariant. Two-dimensional system with the quantum Hall effect geometry and chiral edge states.

Topologically protected surface and edge states are nondegenerate (except for specific points in the Brillouin zone) and helical: states with opposite wave vectors are related through time inversion and have opposite spin projections. Figure 1a shows a two-dimensional topological insulator with helical edge channels (topological insulator with the Z_2 invariant), where the electrons with opposite spin projections move in opposite directions. For comparison, Fig. 1b shows a two-dimensional electron system in a strong magnetic field with quantum Hall effect geometry — an example of a two-dimensional topological insulator with the Z invariant and broken time inversion symmetry. In this case, helical edge channels are formed on the edge of the two-dimensional system and the direction of electron motion in these channels is defined by the direction of the magnetic field [10].

According to the current understanding, the known 3D topological insulators (Z_2 invariant) are some binary and ternary Bi, Sb, Se, Te compounds [11, 12] and strained layers of HgTe [13–16] and α-Sn [17]. An example of two-dimensional topological insulators is quantum wells of a specific width based on HgTe/CdHgTe [18, 19], InAs/GaSb [20] compounds, some heterovalent structures such as InSb/CdTe [21], as well as silicene and germanene — two-dimensional hexagonal crystals of silicon and germanium. Significant efforts are currently focused on studies of different aspects, such as the electronic structure of the surface and edge states in these systems, electric, optical, photoelectric, and thermoelectric properties of topological insulators, topological insulators in a magnetic field or doped with magnetic impurities, and charge carrier transport through the interfaces between topological insulators and ferromagnets or superconductors.

2. Two-dimensional topological insulators based on HgTe/CdHgTe quantum wells

The most impressive experimental results in the physics of two-dimensional topological insulators were obtained in structures with HgTe/CdHgTe quantum wells [22–30].

Bulk cubic HgTe is a material with an inverted band structure, where the Γ_8 band has a higher energy than the Γ_6 band does (Fig. 2a). The inverted positioning of the bands is caused by strong spin-orbit coupling, which splits the Γ_{15} band into Γ_8 and Γ_7 bands and pushes the Γ_8 band above the Γ_6 band. The Fermi level in an undoped crystal goes through the fourfold degenerate point of the Γ_8 band, and the bulk crystal is a gapless semiconductor [31].

The band gap in the charge carrier spectrum can open either due to bulk crystal deformation [13] or due to the size quantization effect in nanoscale structures, like HgTe/CdHgTe quantum wells [18, 32]. The thickness, chemical composition,

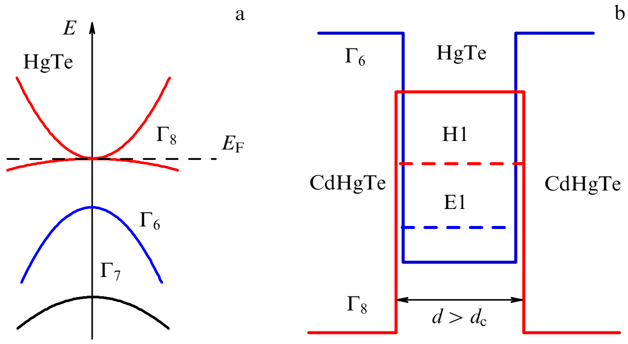

Figure 2. (a) Band structure of the bulk HgTe crystal. (b) Positions of electron E1 and hole H1 subbands resulting from size quantization in HgTe/CdHgTe quantum wells with a thickness exceeding the critical thickness d_c.

and deformation of the quantum well define the ordering of the size quantization subbands and can make the quantum-well structure a trivial or topologically nontrivial insulator, gapless semiconductor, or semimetal. Widely studied quantum wells $Cd_{0.65}Hg_{0.35}Te/HgTe/Cd_{0.65}Hg_{0.35}Te$ on a CdTe substrate have an inverted order for the electron E1 and hole H1 subbands and are two-dimensional topological insulators if well thickness d exceeds some critical thickness $d_c \approx 6.5$ nm, but at the same time is not too large [18, 33]. The band diagram of such structures is illustrated in Fig. 2b.

In the framework of the six-band kp-model, the wave functions of the states in the E1 subband with $\pm 1/2$ spin projection and heavy-hole subband H1 with $\pm 3/2$ momentum projection are defined by the expressions

$$\begin{aligned} |\mathrm{E1}, \pm 1/2\rangle &= f_1(z)|\Gamma_6, \pm 1/2\rangle + f_4(z)|\Gamma_8, \pm 1/2\rangle, \\ |\mathrm{H1}, \pm 3/2\rangle &= f_3(z)|\Gamma_8, \pm 3/2\rangle\,, \end{aligned} \tag{1}$$

where $f_1(z)$, $f_3(z)$, and $f_4(z)$ are smooth envelope functions, z is the structure growth axis, and $|\Gamma_8, \pm 1/2\rangle$, $|\Gamma_8, \pm 3/2\rangle$, and $|\Gamma_6, \pm 1/2\rangle$ are Bloch amplitudes.

The 4×4 effective Hamiltonian describes the states in the quantum well for a nonzero wave vector $\mathbf{k}$ in the interface plane. For symmetric quantum wells with the crystallographic orientation (001) and basis functions $|\mathrm{E1}, +1/2\rangle$, $|\mathrm{H1}, +3/2\rangle$, $|\mathrm{E1}, -1/2\rangle$, and $|\mathrm{H1}, -3/2\rangle$, this Hamiltonian takes the form [18, 34]

$$H = \begin{pmatrix} \delta - Dk^2 & \mathrm{i}Ak_+ & 0 & \mathrm{i}\gamma \\ -\mathrm{i}Ak_- & -\delta - Dk^2 & \mathrm{i}\gamma & 0 \\ 0 & -\mathrm{i}\gamma & \delta - Dk^2 & -\mathrm{i}Ak_- \\ -\mathrm{i}\gamma & 0 & \mathrm{i}Ak_+ & -\delta - Dk^2 \end{pmatrix}, \tag{2}$$

where $\delta = \delta_0 - Bk^2$, $k_\pm = k_x \pm \mathrm{i}k_y$, $x \parallel [100]$, and $y \parallel [010]$ are the axes in the well plane, and A, B, D, δ_0, and γ are the effective Hamiltonian parameters, which can be obtained either from microscopic calculations [37] or from experiment. The parameter δ_0 defines the order of the size quantization subbands and the bandgap energy in the quantum well, $\delta_0 < 0$ for $d > d_c$. The γ parameter describes the mixing of the E1 and H1 states at $\mathbf{k} = 0$ due to the absence of a spatial inversion center in the quantum well. Analysis shows that the mixing mostly takes place at the quantum well interfaces and is quite strong: $2|\gamma| \approx 10$ meV [43]. Mixing-induced anticrossing of the levels leads to a change in the

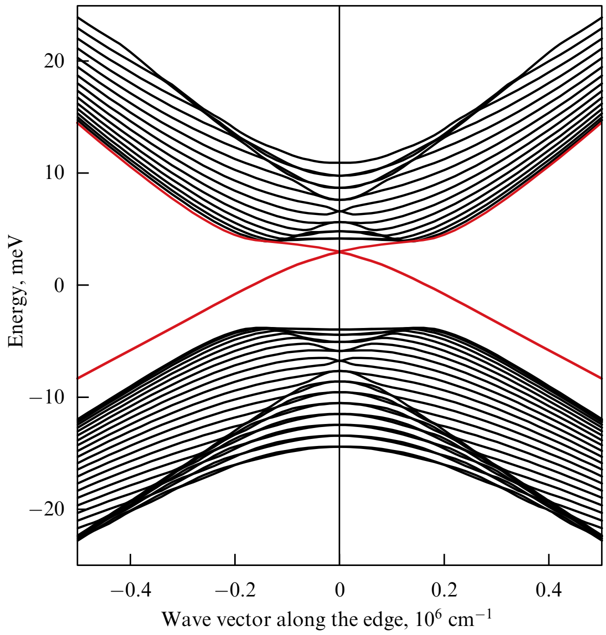

Figure 3. Energy spectrum of electron states in a 1-μm wide strip of an HgTe/CdHgTe quantum well with the inverted subband order [35]. The spectrum contains branches corresponding to helical edge states.

energy spectrum of the 'bulk' and edge states, as well as to strong anisotropy of the effective edge-state g-factor and other effects [35, 36].

Quantum wells with an inverted band structure support one-dimensional helical states along the edges of the sample with wave functions exponentially decaying inside the quantum well (see Fig. 1a). The dispersion and the wave functions of the edge states can be found from the Schrödinger equation $H\Psi = E\Psi$ with appropriate boundary conditions.

Figure 3 displays the spectrum of electron states in an HgTe/CdHgTe quantum well calculated for open boundary conditions ($\Psi = 0$ at the quantum well edge). Aside from the 'bulk' states that are delocalized in the well plane, the spectrum contains two branches, which are located in the bandgap of the bulk states and describe the helical edge states. In the vicinity of the branch intersection, the edge state spectrum is linear and can be described with the effective Weyl's Hamiltonian

$$H_{\text{edge}} = \hbar v_{\text{edge}} \sigma_z k \,, \tag{3}$$

where v_{edge} is the velocity, σ_z the Pauli matrix, and k the wave vector along the edge. The influence of the boundary conditions on the spectrum and the wave functions of the edge states was studied in paper [38].

Starting with pioneering study [19], the charge carrier transport in topologically nontrivial HgTe/CdHgTe quantum wells was studied experimentally in a number of papers (see, for example, Refs [22, 23, 25–28]). It was shown that the edge channels make a strong contribution to the conductivity and form a nonlocal response. At the same time, it was discovered that the ballistic character of the charge carrier motion along the edge channels is observed only on micrometer scales, while in larger samples the transport demonstrates a diffusive character. Such behavior contradicts the simple model of helical edge states, in which the process of electron back-scattering on electrostatic potential fluctuations with spin flip is forbidden. This means that the topological protection of the states, which stems from the time-inversion symmetry, is violated in real samples. Experimental investigations of the magnetic field influence on the edge channel transport are even more intriguing: the first papers claimed that the transport is suppressed by the magnetic field [37], but more detailed investigations have shown that the magnetoresistance is nonmonotonic [39], and the suppression takes place only in large fields [25].

The microscopic mechanisms of the observed momentum and spin relaxation in the edge channels are currently under discussion. Violation of the ballistic character of electron motion can be associated with scattering on magnetic impurities, which can occasionally appear in the structure [40–43]. The scattering can also take place on the spin polarization fluctuations of the atomic nuclei in the crystal lattice due to hyperfine coupling [44–46]. The most probable mechanism for ballistic transport suppression in real structures is the interaction between the electrons in the edge channels and electron or hole 'puddles', which are formed near the sample edges due to potential fluctuations [47]. In this case, one could expect that improvement in the topological insulator fabrication technology will lead to an increase in the electron mean free path in the edge channels.

An effective instrument for the investigation of symmetry and spin structure of states together with the charge carrier kinetic parameters is the measurement of photogalvanic effects — the generation of a directed electrical current induced by optical transitions. In topological insulators, the edge-state photogalvanic effects can be experimentally separated from the bulk ones, because, unlike the latter, they also appear when the energy of the exciting photon $\hbar\omega$ is lower than the bandgap energy. Additional information on the nature of photocurrent is given by its polarization dependence, which is usually different for edge and bulk contributions to the photocurrent.

Depending on the photon energy, bandgap energy, and the Fermi level position, the edge photogalvanic effects can be induced by different types of optical transitions (Fig. 4a). Direct optical transitions between the edge states with opposite spin projections are possible if $\hbar\omega > 2|E_{\text{F}}|$, where E_{F} is the Fermi energy with respect to the Weyl point. Such transitions are allowed in the magnetic dipole approximation [48] and in the electric dipole approximation with the spatial

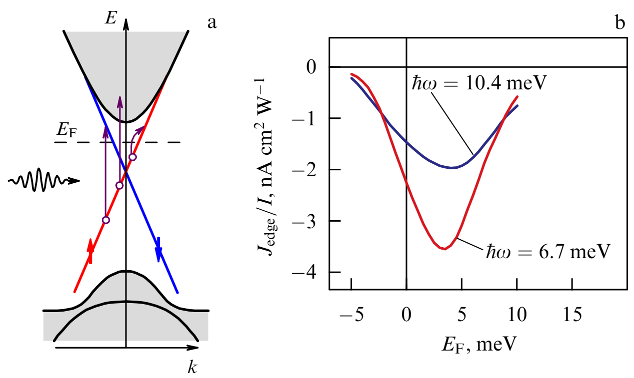

Figure 4. (a) Band diagram of electron states in a two-dimensional topological insulator. Vertical arrows indicate possible optical transitions from the edge states. (b) Dependences of the photocurrent induced by edge-state photoionization with the circularly polarized radiation on the Fermi energy, calculated for various photon energies [29].

asymmetry of the structure taken into account [49]. Direct optical transitions in the electric dipole approximation can also appear between the edge and bulk states of the conduction or valence bands [50]. Finally, high-frequency radiation absorption may be related to indirect optical transitions involving impurities or phonons [51, 52]. The latter need to take into account the nonlinearity of the spectrum, virtual processes with intermediate states in the conduction or valence band, or electron scattering with a spin-flip.

Edge photocurrents generated in topological insulators based on HgTe/CdHgTe quantum wells were observed in paper [29] in absorption of terahertz radiation, with the photon energy being lower than the bandgap. The photocurrent flowed in opposite directions on opposite edges of the sample, and its direction was defined by the sign of the circular polarization of radiation. Analyses of both the photocurrent dependence on the structure gate voltage V_g and the efficiency of various mechanisms for current generation have shown that in a certain gate voltage (V_g) range the photocurrent is induced by the photoionization of the edge states into the conduction band. With the absorption of circularly polarized radiation, for example, with σ^+ polarization, the probability of optical transitions from the edge state branch with $s = +1/2$ spin projection is higher than that for the branch with $s = -1/2$. Since the spin projection in edge states is locked with the momentum direction, the spin-dependent asymmetry of the optical transitions leads to the generation of electric current along the sample edge. If the sign of the circular polarization is changed, the asymmetry of the optical transitions will change too, and the photocurrent will flow in the opposite direction.

In the relaxation time approximation, the photocurrent flowing through the edge states is defined by the expression

$$J_{\mathrm{edge}} = -e \sum_{ks} \tau_{\mathrm{p}}(\varepsilon_{ks})\, v_{ks}\, g_{ks}\,, \tag{4}$$

where e is the electron charge, τ_{p} the electron momentum relaxation time, which is defined by backscattering processes, ε_{ks} and $v_{ks} = (1/\hbar)\, \mathrm{d}\varepsilon_{ks}/\mathrm{d}k$ are the energy and the velocity, and g_{ks} is the rate of optical transitions from the state with wave vector k and spin projection s. It is assumed that the electron spin relaxation is quite fast in the bulk, so that the photoionized electrons lose their spin orientation before falling back into the edge states.

The spin-dependent asymmetry of the optical transitions described above can be expressed in the following form:

$$\frac{g_{k,+1/2} - g_{-k,-1/2}}{g_{k,+1/2} + g_{-k,-1/2}} = KP_{\mathrm{circ}}\,, \tag{5}$$

where K is the dimensionless parameter describing the selection rule strictness, and P_{circ} is the degree of the circular polarization. Calculations show that the K parameter only weakly depends on the wave vector k and the photon energy [29]. In the framework of a simple four-subband model, which does not take into account state mixing at the quantum well interfaces, the K parameter at $k = 0$ equals $2BD/(B^2 + D^2)$, where B and D are the Hamiltonian parameters (2); see paper [50]. This allows rewriting the expression for the edge photocurrent (4) as

$$J_{\mathrm{edge}} = -\frac{eKP_{\mathrm{circ}}}{2\pi\hbar} \int \tau_{\mathrm{p}}(\varepsilon)\, g_{\mathrm{tot}}(\varepsilon)\, \mathrm{d}\varepsilon\,, \tag{6}$$

where $g_{\mathrm{tot}}(\varepsilon) = g_{k,+1/2} + g_{-k,-1/2}$ is the full-rate electron photoionization by circularly polarized radiation from the edge states with energy $\varepsilon = \varepsilon_{ks}$.

Figure 4b shows the edge-state photoionization-induced photocurrent dependences on the Fermi level position, which can be controlled in the experiment by tuning the gate voltage. The curves are calculated for two photon energies $\hbar\omega$ corresponding to experiment [29]. The effective Hamiltonian parameters were taken from Ref. [37], the electron relaxation time in the edge channel $\tau_{\mathrm{p}} = 20$ ps was estimated from the mean free path of ~ 7 μm, as observed in the structure, and the velocity $v_{\mathrm{edge}} \sim 10^7$ cm s^{-1}. The dependences were calculated without fitting parameters and agree quite well with the experimental data.

3. Three-dimensional topological insulators based on strained HgTe films

The surface of three-dimensional topological insulators supports two-dimensional conducting states with a strong correlation between the momentum direction and the spin orientation. Since the time inversion symmetry does not forbid electron scattering on the electrostatic potential at an arbitrary angle (it is only the exact backscattering which is forbidden as a transition between the states connected through the time inversion operation), electron transport along the helical states usually has a diffusive character.

In topological insulators based on bismuth and antimony selenides and tellurides, the bandgap energy can reach several hundred millielectron-volts, but the surface charge carrier mobility is not high even at low temperatures, so studies of electron transport along the surface states is often complicated due to high charge carrier concentration in the bulk [53–57]. For such structures, the conventional experimental method for surface state detection and measurement of their energy spectrum is an angle resolved photoelectron spectroscopy (ARPES) [12].

In topological insulators based on strained epitaxial HgTe films, the bandgap energy of ~ 20 meV in the bulk state spectrum opens due to deformation. The surface carrier mobility in these systems reaches $\sim 10^5$ cm^2 $\mathrm{V}^{-1}\,\mathrm{s}^{-1}$, which allows observing the quantum Hall effect and Shubnikov–de Haas oscillations [14, 15]. The high mobility of the surface carriers and an insignificant contribution of the bulk carriers also allow studying the cyclotron resonance in the transmission spectra and the magneto-optical Faraday effect [58, 59].

Figure 5 shows the spectrum of electron states in the CdHgTe/HgTe/CdHgTe structure with an 80-nm thick strained HgTe film. The calculation is performed in the framework of the six-band kp-model for structures with (013) crystallographic orientation, which are often studied experimentally. The spectrum contains branches of the surface states in the bandgap of the bulk strained HgTe film, and these states are localized near the upper and lower boundaries of the film. Weyl points of the surface states for the upper and lower film surfaces are located deep in the valence band, which causes mixing between surface and bulk states and deviation of the dispersion of the surface states from the linear dependence [14, 16]. In structures with (013) crystallographic orientation, the spectrum is anisotropic in the interface plane. Dispersions of surface and bulk states for two orthogonal directions of the wave vector k are shown with solid and dashed lines.

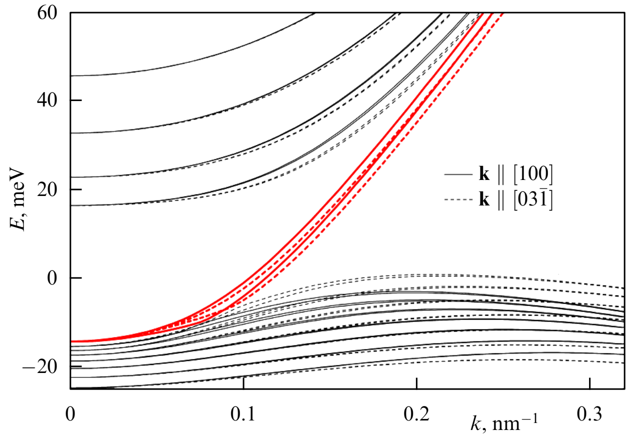

Figure 5. Energy spectrum of electron states in the $Cd_{0.65}Hg_{0.35}Te$/$HgTe$/$Cd_{0.65}Hg_{0.35}Te$ structure grown on CdTe substrate with (013) crystallographic orientation. The strained HgTe film thickness is 80 nm, and the transverse electric field is $E_z = 0.5$ kV cm^{-1} [16].

A wonderful opportunity to study both the surface states in three-dimensional topological insulators and edge states in two-dimensional topological insulators is given by photogalvanic and the second-harmonic generation effects. Experimental and theoretical studies of surface photogalvanic effects were performed for three-dimensional topological insulators, such as Bi_2Se_3, Bi_2Te_3, Sb_2Te_3, $(Bi_{1-x}Sb_x)_2Te_3$, and $(Bi_{1-x}In_x)_2Se_3$ in papers [60–68], and for topological insulators based on strained HgTe films in paper [16]. The measurements allowed reconstructing the charge carrier spectrum and investigating the photocurrent generation mechanism for various wavelength ranges. In topological insulators based on HgTe films, the photogalvanic effect was studied in the external magnetic field normal to the film surface. A significant increase in the photocurrent was observed under cyclotron resonance conditions, when the electromagnetic field frequency is close to the cyclotron frequency of the surface charge carriers [16]. The calculated spectrum well describes the observed positions of the cyclotron resonances.

The physics of topological insulators is currently actively developing and without a doubt will be very fruitful both for fundamental science and for practical applications in electronics and optoelectronics.

Acknowledgments

The author is grateful to M V Durnev, G V Budkin, and S D Ganichev for helpful discussions. The work was performed with the financial support of the Russian Science Foundation (project 17-12-01265).

References

1. Berezinskii V L *Sov. Phys. JETP* **34** 610 (1972); *Zh. Eksp. Teor. Fiz.* **61** 1144 (1971)
2. Kosterlitz J M, Thouless D J *J. Phys. C* **6** 1181 (1973)
3. Thouless D J et al. *Phys. Rev. Lett.* **49** 405 (1982)
4. Haldane F D M *Phys. Rev. Lett.* **61** 2015 (1988)
5. Hasan M Z, Kane C L *Rev. Mod. Phys.* **82** 3045 (2010)
6. Qi X-L, Zhang Sh-Ch *Rev. Mod. Phys.* **83** 1057 (2011)
7. Tamm I *Phys. Z. Sowjetunion* **1** 733 (1932)
8. Volkov B A, Pankratov O A *JETP Lett.* **42** 178 (1985); *Pis'ma Zh. Eksp. Teor. Fiz.* **42** 145 (1985)
9. Volkov B A, Pankratov O A *Sov. Phys. Usp.* **29** 575 (1986); *Usp. Fiz. Nauk* **149** 334 (1986)
10. Dolgopolov V T *Phys. Usp.* **57** 105 (2014); *Usp. Fiz. Nauk* **184** 113 (2014)
11. Zhang H et al. *Nature Phys.* **5** 438 (2009)
12. Xia Y et al. *Nature Phys.* **5** 398 (2009)
13. Fu L, Kane C L *Phys. Rev. B* **76** 045302 (2007)
14. Brüne C et al. *Phys. Rev. Lett.* **106** 126803 (2011)
15. Kozlov D A et al. *Phys. Rev. Lett.* **112** 196801 (2014)
16. Dantscher K-M et al. *Phys. Rev. B* **92** 165314 (2015)
17. Barfuss A et al. *Phys. Rev. Lett.* **111** 157205 (2013)
18. Bernevig B A, Hughes T L, Zhang S-C *Science* **314** 1757 (2006)
19. König M et al. *Science* **318** 766 (2007)
20. Knez I et al. *Phys. Rev. Lett.* **112** 026602 (2014)
21. Liu Q et al. *Adv. Function. Mater.* **26** 3259 (2016)
22. Roth A et al. *Science* **325** 294 (2009)
23. Gusev G M et al. *Phys. Rev. B* **84** 121302(R) (2011)
24. Zholudev M et al. *Phys. Rev. B* **86** 205420 (2012)
25. Ma E et al. *Nature Commun.* **6** 7252 (2015)
26. Min'kov G M et al. *JETP Lett.* **101** 469 (2015); *Pis'ma Zh. Eksp. Teor. Fiz.* **101** *522 (2015)*
27. Tikhonov E S et al. *JETP Lett.* **101** 708 (2015); *Pis'ma Zh. Eksp. Teor. Fiz.* **101** 787 (2015)
28. Kononov A et al. *JETP Lett.* **101** 41 (2015); *Pis'ma Zh. Eksp. Teor. Fiz.* **101** 44 (2015)
29. Dantscher K-M et al. *Phys. Rev. B* **95** 201103(R) (2017)
30. Kadykov A M et al. *Phys. Rev. Lett.* **120** 086401 (2018)
31. D'yakonov M I, Khaetskii A V *JETP Lett.* **33** 110 (1981); *Pis'ma Zh. Eksp. Teor. Fiz.* **33** 115 (1981)
32. Gerchikov L G, Subashiev A V *Sov. Phys. Semicond.* **23** 1368 (1989); *Fiz. Tekh. Poluprovodn.* **23** 2210 (1989)
33. Raichev O E *Phys. Rev. B* **85** 045310 (2012)
34. Tarasenko S A et al. *Phys. Rev. B* **91** 081302(R) (2015)
35. Durnev M V, Tarasenko S A *Phys. Rev. B* **93** 075434 (2016)
36. Minkov G M et al. *Phys. Rev. B* **93** 155304 (2016)
37. König M et al. *J. Phys. Soc. Jpn.* **77** 031007 (2008)
38. Enaldiev V V, Zagorodnev I V, Volkov V A *JETP Lett.* **101** 89 (2015); *Pis'ma Zh. Eksp. Teor. Fiz.* **101** 94 (2015)
39. Gusev G M et al. *Phys. Rev. B* **87** 081311(R) (2013)
40. Tanaka Y, Furusaki A, Matveev K A *Phys. Rev. Lett.* **106** 236402 (2011)
41. Lunde A M, Platero G *Phys. Rev. B* **86** 035112 (2012)
42. Altshuler B L, Aleiner I L, Yudson V I *Phys. Rev. Lett.* **111** 086401 (2013)
43. Kurilovich P D et al. *JETP Lett.* **106** 593 (2017); *Pis'ma Zh. Eksp. Teor. Fiz.* **106** 575 (2017)
44. Maestro A D, Hyart T, Rosenow B *Phys. Rev. B* **87** 165440 (2013)
45. Lunde A M, Platero G *Phys. Rev. B* **88** 115411 (2013)
46. Tarasenko S A, Burkard G *Phys. Rev. B* **94** 045309 (2016)
47. Väyrynen J I et al. *Phys. Rev. B* **90** 115309 (2014)
48. Dóra B et al. *Phys. Rev. Lett.* **108** 056602 (2012)
49. Durnev M V, Tarasenko S A *J. Phys. Condens. Matter* **31** 035301 (2019)
50. Kaladzhyan V, Aseev P P, Artemenko S N *Phys. Rev. B* **92** 155424 (2015)
51. Tarasenko S A *JETP Lett.* **85** 182 (2007); *Pis'ma Zh. Eksp. Teor. Fiz.* **85** 216 (2007)
52. Entin M V, Magarill L I *JETP Lett.* **103** 711 (2016); *Pis'ma Zh. Eksp. Teor. Fiz.* **103** 804 (2016)
53. Checkelsky J G et al. *Phys. Rev. Lett.* **103** 246601 (2009)
54. Analytis J G et al. *Phys. Rev. B* **81** 205407 (2010)
55. Ren Z et al. *Phys. Rev. B* **84** 165311 (2011)
56. Xia B et al. *Phys. Rev. B* **87** 085442 (2013)
57. Pan Y et al. *New J. Phys.* **16** 123035 (2014)
58. Shuvaev A et al. *Appl. Phys. Lett.* **102** 241902 (2013)
59. Shuvaev A M et al. *Phys. Rev. B* **87** 121104(R) (2013)
60. Hsieh D et al. *Phys. Rev. Lett.* **106** 057401 (2011)
61. McIver J W et al. *Nature Nanotechnol.* **7** 96 (2012)
62. Olbrich P et al. *Phys. Rev. Lett.* **113** 096601 (2014)
63. Shikin A M et al. *Phys. Solid State* **58** 1675 (2016); *Fiz. Tverd. Tela* **58** 1617 (2016)
64. Hamh S Y et al. *Phys. Rev. B* **94** 161405(R) (2016)
65. Galeeva A V et al. *Semicond. Sci. Technol.* **31** 095010 (2016)
66. Pan Y et al. *Nature Commun.* **8** 1037 (2017)
67. Huang Y Q et al. *Nature Commun.* **8** 15401 (2017)
68. Kuroda K et al. *Phys. Rev. B* **95** 081103(R) (2017)